Electronic Supplementary Information

Interstitial oxygen defect induced mechanoluminescence in $KCa(PO_3)_3$:Mn^{2+}

Huimin Chen,[a] Yuxing Bai,[a] Lirong Zheng,[b] Li Wu,*[a] Liwei Wu,[a] Yongfa Kong,[a] Yi Zhang *[c] and Jingjun Xu [a]

[a]Key Laboratory of Weak-Light Nonlinear Photonics, Ministry of Education, School of Physics, Nankai University, Tianjin 300071, China. E-mail: *lwu@nankai.edu.cn.

[b]Multi-Discipline Research Center, Institute of High Energy Physics, Chinese Academy of Sciences, Beijing 100049, China.

[c]College of Electronic Information and Optical Engineering and Tianjin Key Laboratory of Photo-electronic Thin Film Devices and Technology, Nankai University, Tianjin 300071, China. E-mail: *yizhang@nankai.edu.cn.

Material preparation and characterization

Materials and synthesis: A series of solid solutions of $KCa_{1-y}Mg_y(PO_3)_3$:Mn^{2+} were synthesized *via* a high-temperature solid-state method. Analytical purity K_2CO_3, $CaCO_3$, MgO, $NH_4H_2PO_4$ and MnO_2 were ground and sintered at 600 °C for 6 h and 815 °C for 12 h in the ambient atmosphere with an intermediate grinding step in between the two sintering processes. Finally, the sintered products were well ground after cooling to room temperature.

Characterization: The XRD patterns were collected on an X-ray diffractometer (X'Pert Pro, PANalytical B.V., Netherlands) and the structural refinements were collected over a 2θ range from 10° to 120° at intervals of 0.017°. Scanning electron microscopy (SEM, SU8020, HITACHI, Japan) with energy dispersive X-ray spectroscopy (EDS, EMAX, HORIBA) was used to characterize the morphologies of the powder samples. The XPS spectra were obtained using a Thermo Scientific ESCALAB 250Xi (America) and calibrated to a C 1s electron peak at 284.8 eV. The XAFS spectra were tested *via* the 1W1B beam line (Beijing Synchrotron Radiation Facility). The PLE and PL spectra were measured by a spectrofluorometer (FLS920, Edinburgh Instruments, England). The diffuse reflectance spectra were collected by a UV/Vis/NIR spectrophotometer (Cary5000, America). A grating spectrometer (ANDOR,

Kymera 328i, England) was used to collect the ML spectra. After irradiating with 365 nm UV light for 10 min, the TL curves of the powder samples were obtained using a thermoluminescence meter (FJ427A1, CNCS, China).

Computational methods: All the DFT calculations were implemented with the Vienna ab initio simulation package (VASP). The electron–ion interactions were determined using the projector augmented wave pseudo-potential method.[1] K ($3s^2 3p^6 4s^1$), Ca ($3p^6 4s^2$), Mg ($3s^2$), P ($3s^2 3p^3$), O ($2s^2 2p^4$) and Mn ($3d^6 4s^1$) electrons were treated as their own valence electrons. To investigate the density of states accurately, the spin-polarized generalized gradient approximation[2] with the Perdew–Burke–Ernzerhof[3] functional was adopted to describe the electronic exchange–correlation potential. The cutoff energy of 400 eV was used for the plane-wave basis set to expand the pseudo valence wave function. A $2 \times 2 \times 1$ supercell was constructed, in which Ca ions were substituted by Mn and Mg ions. Moreover, k-point grids for the Brillouin zone were generated with $9 \times 9 \times 6$ and $1 \times 1 \times 1$ G-centered models for the primitive cell and supercell, respectively. All the optimization processes were considered to satisfy the convergence criterion when the total energy change was less than 1×10^{-4} eV per step, and the maximum force was less than 5×10^{-2} eV Å^{-1} per atom.
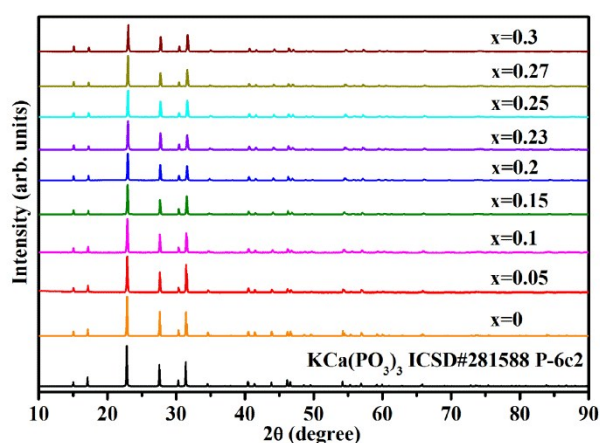

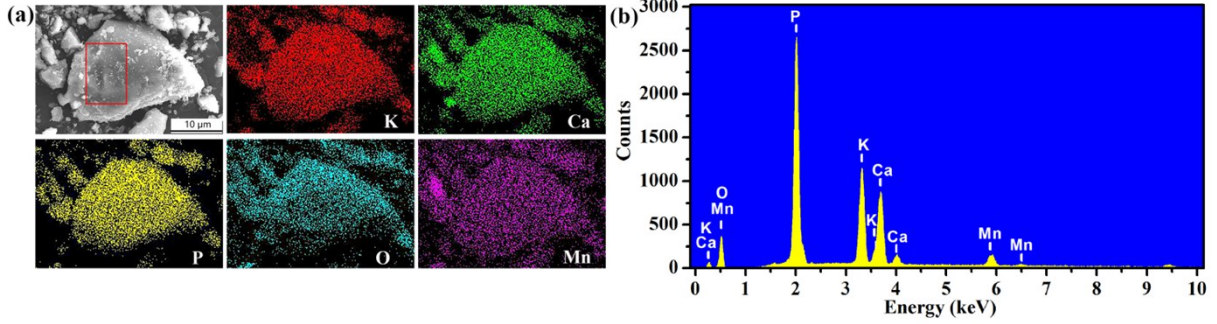**Fig. S1** The XRD patterns of KCPO:xMn^{2+}.

Fig. S2 (a) SEM image and elemental mapping images of KCPO:0.23Mn^{2+}. (b) EDS analysis of KCPO:0.23Mn^{2+} detected in the selected square area in (a).

PLE and PL spectra of KCPO:Mn are measured, as shown in Fig. 1c. The excitation spectra from 300–460 nm can be ascribed to Mn^{2+} d–d transitions. The narrow band centered at 341 nm comes from $^6A_1$–$^4E(^4D)$ transition. The peaks from 326 to 370 nm originate from $^6A_1$–$^4T_2(D)$ transition. The peaks centered at 382 nm, 400 nm, and 427 nm are from the Mn^{2+} transition of $^6A_1$–$^4A_1,^4E(^4G)$, $^6A_1$–$^4T_2(^4G)$, and $^6A_1$–$^4T_1(^4G)$.[4] Monitored at different excitation wavelengths, the emission spectra show broad yellow bands with the center of 578 nm, which is attributed to the transition from $^4T_1(^4G)$ to $^6A_1(^6S)$ of Mn^{2+} ions.[5] The emission intensity increases with Mn^{2+} ions concentration until reaching the maximum of $x = 0.23$, then the emission intensity decreases when $x > 0.23$, as shown in Fig. S3. As Mn^{2+} ions increase, the distance between them decreases. The following equation is used to calculate the critical distance (R_c):[6]

$$R_c = 2\left[\frac{3V}{4\pi x_c N}\right]^{1/3}$$

(1)

where V refers to the unit cell volume, x_c is the critical concentration of Mn^{2+}, and N represents the number of cation sites in each unit cell. For KCPO:xMn^{2+}, $V = 416.608$ Å^3, $x_c = 0.23$, N = 2, $R_c = 12$ Å, which greater than 5 Å, indicating that the concentration quenching is caused by multi-polar interaction. Based on Dexter's theory, the interaction type is represented by the following equation:[7]

$$\frac{I}{x} = \frac{K}{1 + \beta(x)^{\frac{\theta}{3}}}$$

(2)

where I denotes the emission intensity, x is the concentration of activator ions, β and K are constants. $\theta = 6, 8, 10$ refers to the dipole–dipole, dipole–quadrupole, and quadrupole–quadrupole interaction mechanism, respectively. According to the slope value of −3.184 from

the inset, the obtained θ value is 9.55, which is close to 10, indicating that the concentration quenching of KCPO:xMn^{2+} is caused by quadrupole–quadrupole interaction.[5]

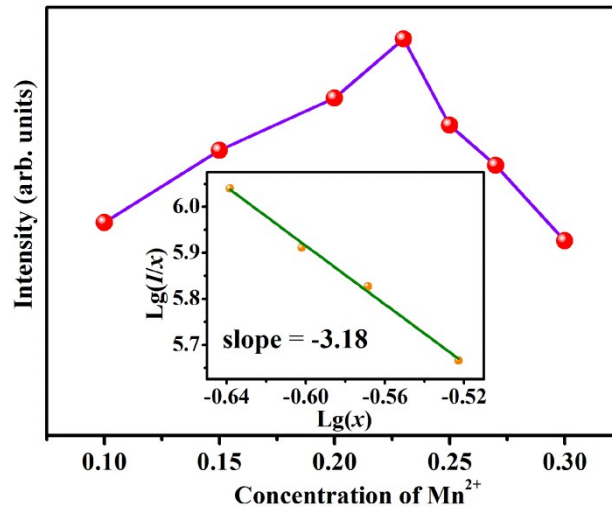**Fig. S3** The emission intensity versus Mn^{2+} concentration of KCPO:xMn^{2+}. The inset is the relationship between lg(I/x) and lg(x).

Fig. S4 shows the ultraviolet-visible diffuse reflectance spectra of KCPO:0.23Mn^{2+}. The decreasing reflectance from 200 to 400 nm is attributed to the host absorption.[8] The absorption occurred at about 400–650 nm belongs to the self-trapped exciton emission from the laser experiment.[9] The band gap E_g is determined by the Kubelka-Munk equation:[10]

$$[F(R_\infty)hv]^n = A(hv - E_g) \tag{3}$$

where hv represents the photon energy, A is the proportional constant, and $n = 2$ denotes the direct allowed transition. The Kubelka-Munk absorption coefficient $F(R_\infty)$ is calculated according to the following equation:

$$F(R_\infty) = (1 - R)^2/2R \tag{4}$$

According to the DFT calculations, the KCPO matrix belongs to the direct energy band structure, thus the curves of $[F(R_\infty)hv]^2$ to hv are plotted and E_g is obtained by extrapolating the linear portion of the plot to $[F(R_\infty)hv]^2 = 0$. As shown in the insets of Fig. S4, the optical band gap value of KCPO:0.23Mn^{2+} is 5.45 eV.
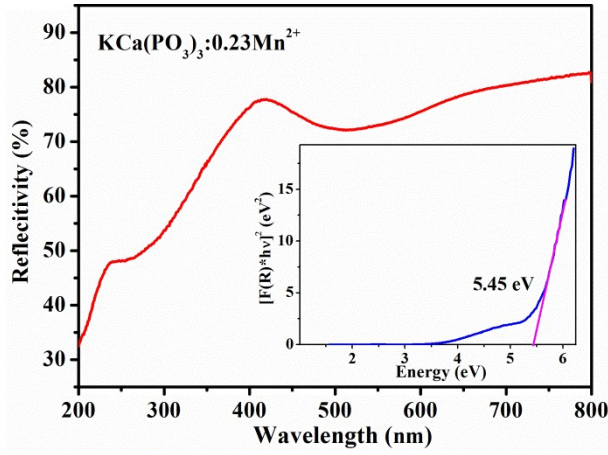
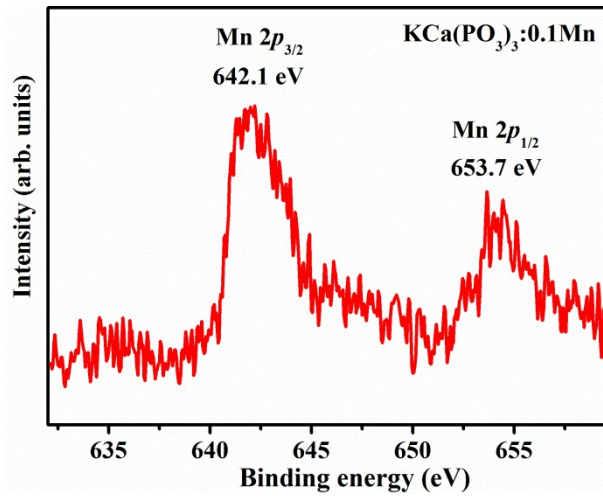**Fig. S4** The ultraviolet-visible diffuse reflectance spectra of KCPO:0.23Mn^{2+}.

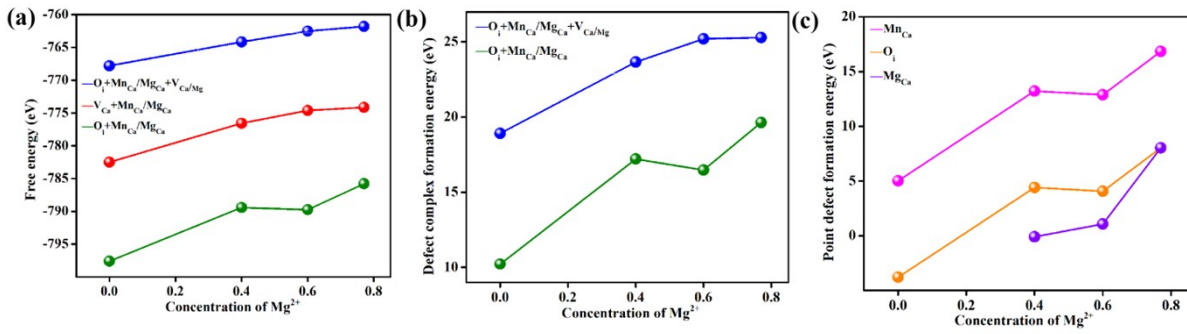**Fig. S5** The high-resolution XPS peaks of Mn 2p of KCPO:0.1Mn^{2+}.

Fig. S6 (a) The total energies with various types of defect complexes versus different Mg^{2+} concentration. (b, c) The formation energies of defect complexes and point defects versus different Mg^{2+} concentration.
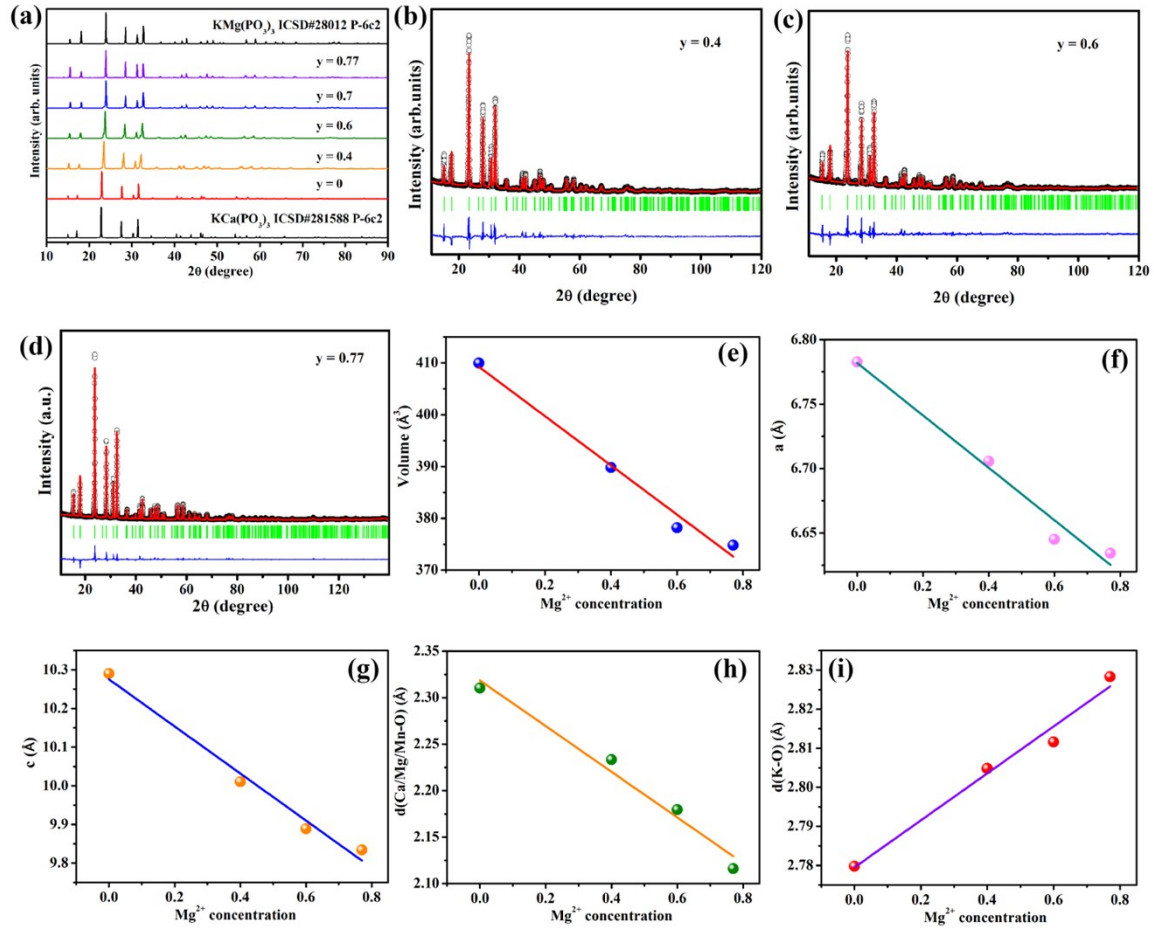
5

Fig. S7 (a) The XRD patterns of KCMPO:0.23Mn^{2+}. (b–d) Rietveld refinement results of KCMPO:0.23Mn^{2+} at y = 0.4, 0.6, and 0.77. The small black circles and red continuous lines represent the experimental and the calculated values respectively; the green vertical bars depict the position of Bragg peaks; the blue trace indicates the difference between the experimental and the calculated intensity values. (e–g) Dependence of the cell volume and cell parameters on y in KCMPO:0.23Mn^{2+} (y = 0, 0.4, 0.6, and 0.77). (h, i) The dependence of d(Ca/Mg/Mn–O) and d(K–O) bond length on Mg^{2+} concentration.
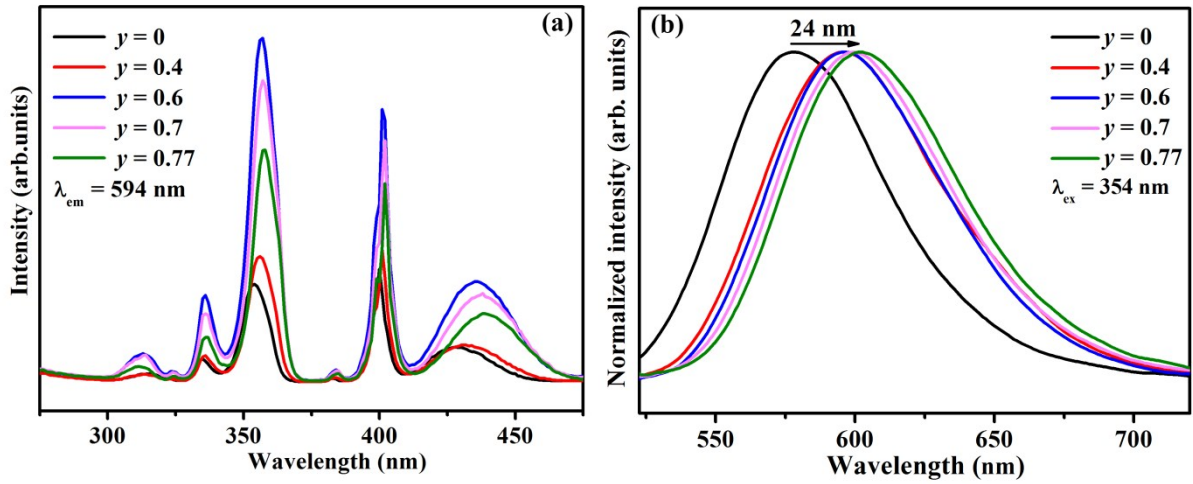
Fig. S8 (a) The PLE spectra of KCMPO:0.23Mn^{2+}. (b) The normalized PL spectra of KCMPO:0.23Mn^{2+}.
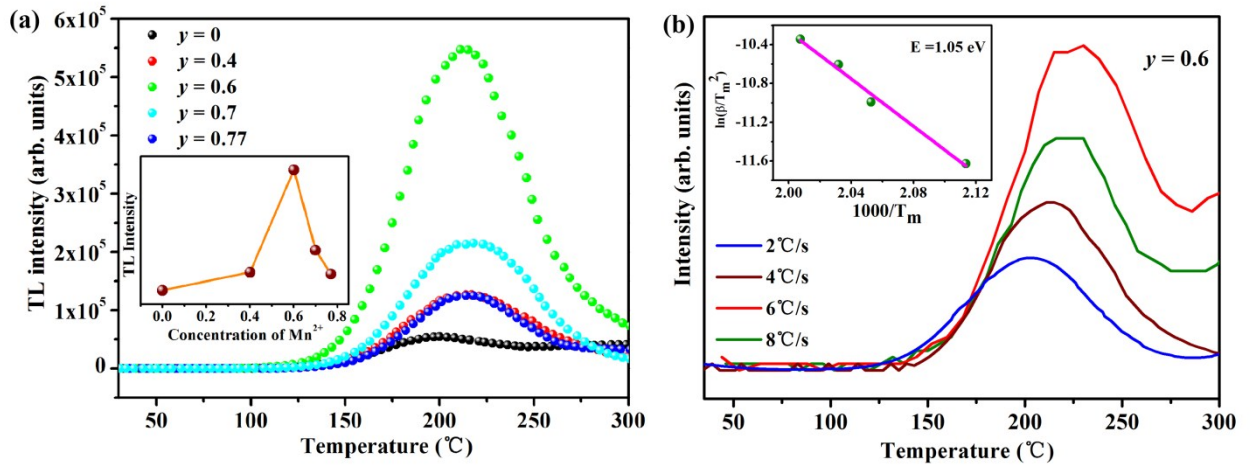

Fig. S9 (a) The TL curves of KCMPO:0.23Mn^{2+} (y = 0, 0.4, 0.6, 0.7, 0.77) at the heating rate of 4 °C/s. (b) TL curves of KC$_{0.17}$M$_{0.6}$PO:0.23Mn^{2+} at different heating rate and the Hoogenstraaten plots.
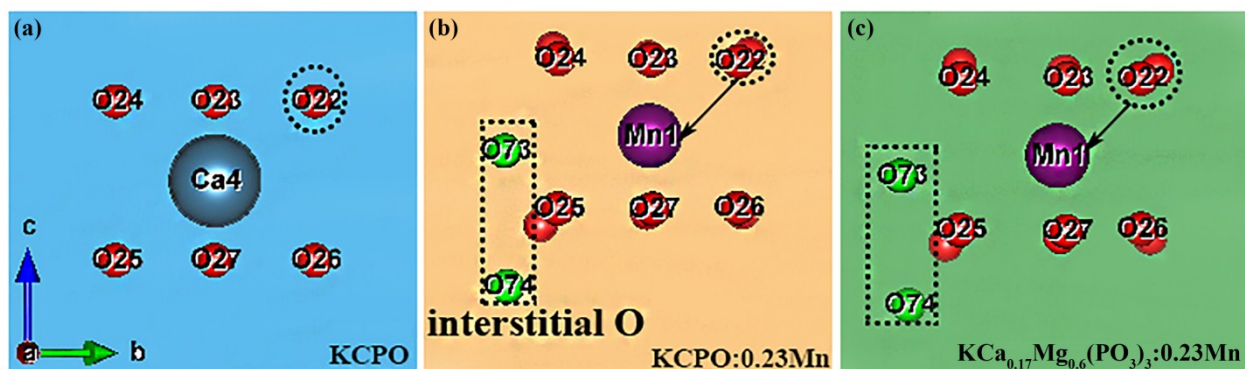
Fig. S10 The optimized local atomic arrangement structures around Mn of KCMPO:0.23Mn^{2+} (y = 0, 0.4, 0.6, 0.77).

Table S1 Lattice parameters and agreement factors for KCMPO:0.23Mn^{2+} refined by Rietveld method.

Samples	y = 0	y = 0.4	y = 0.6	y = 0.77
Crystal system	Hexagonal	Hexagonal	Hexagonal	Hexagonal
Space group	P-6c2	P-6c2	P-6c2	P-6c2
a/Å	6.7827(1)	6.7056(3)	6.6454(2)	6.6344(1)
c/ Å	10.2905(1)	10.0104(5)	9.8889(2)	9.8340(1)
V/Å^3	409.9846(2)	389.8139(3)	378.1975(2)	374.8511(3)
Z	2	2	2	2
d(Ca/Mg/Mn–O)	2.3104(3)	2.2334(4)	2.1795(4)	2.1162(1)
d(K–O)	2.7798(3)	2.8048(5)	2.8116(4)	2.8283(1)
Diffractometer	X'Pert Pro, PANalytical	X'Pert Pro, PANalytical	X'Pert Pro, PANalytical	X'Pert Pro, PANalytical
Radiation type	Cu-Kα	Cu-Kα	Cu-Kα	Cu-Kα
Wavelength (Å)	1.5406	1.5406	1.5406	1.5406
Profile range (°2θ)	11.01–120	11.01–120	11.01–120	11.01–120
Step size (°2θ)	0.017	0.017	0.017	0.017
No. observation (N)	7941	7941	8000	7941
No. contribution reflections (Kα1 + Kα2)	676	676	646	614
No. structure parameters (P_1)	17	17	17	17
No. profile parameters (P_2)	13	12	12	11
R$_p$ (%)	5.42	7.17	6.86	5.58
R$_{wp}$ (%)	7.00	9.78	9.02	7.31
R$_{exp}$ (%)	3.96	3.06	3.08	3.82
R$_{Bragg}$ (%)	7.04	9.65	9.50	9.48

Table S2 Refinement atomic positions for KCMPO:0.23Mn^{2+}.

Samples	$y = 0$	$y = 0.4$	$y = 0.6$	$y = 0.77$
Ca (2c)				
x	1/3	1/3	1/3	-
y	2/3	2/3	2/3	-
z	0	0	0	-
Occupancy	0.7472 (1)	0.3700 (1)	0.1701 (1)	-
Mg (2c)				
x	-	1/3	1/3	1/3
y	-	2/3	2/3	2/3
z	-	0	0	0
Occupancy	-	0.3925 (2)	0.5826 (1)	0.7557 (1)
Mn (2c)				
x	1/3	1/3	1/3	1/3
y	2/3	2/3	2/3	2/3
z	0	0	0	0
Occupancy	0.2528 (1)	0.2375 (1)	0.2473 (2)	0.2443 (2)
K (2e)				
x	2/3	2/3	2/3	2/3
y	1/3	1/3	1/3	1/3
z	0	0	0	0
Occupancy	1.0000	1.0000	1.0000	1.0000
P (6k)				
x	0.7298 (4)	0.2262 (7)	0.2226 (6)	0.2246 (3)
y	0.9602 (4)	-0.0488 (9)	-0.0540 (8)	-0.0570 (3)
z	3/4	1/4	1/4	1/4
Occupancy	1.0000	1.0000	1.0000	1.0000
O1 (6k)				
x	0.8066 (7)	0.2452 (16)	0.2513 (15)	0.2396 (8)
y	0.7668 (8)	0.1933 (11)	0.1867 (13)	0.1901 (7)
z	3/4	1/4	1/4	1/4
Occupancy	1.0000	1.0000	1.0000	1.0000
O2 (12l)				
x	0.6175 (5)	0.3206 (9)	0.3176 (8)	0.3212 (4)
y	0.9481 (7)	-0.0640 (8)	-0.0714 (7)	-0.0800 (0)
z	0.8748 (2)	1/8	1/8	1/8
Occupancy	1.0000	1.0000	1.0000	1.0000

Table S3 The charge numbers of Mn ions for KCPO:0.23Mn^{2+}.

KCPO:0.23Mn^{2+}	Original Valence Electron	Remaning Valence Electron	Transfer Electron
Mn1	7	5.2931	1.7069
Mn2	7	5.2973	1.7027

Table S4 The XPS elemental analysis of KCPO:0.23Mn^{2+}.

Element	K	Ca	P	O	Mn
Theory (%)	12.24	9.66	29.08	45.07	3.95
XPS value (%)	11.67	9.01	23.38	52.27	3.67

Table S5 The total Helmholtz free energies and formation energies of KCPO:0.23Mn^{2+} with different kinds of defects.

Samples	$E_{\text{tot-imperfect}}$ (eV)			E_f (eV)			
				Defect Complex		Point Defect	
	$V_{Ca}+Mn_{Ca}$	O_i+Mn_{Ca}	$O_i+Mn_{Ca}+V_{Ca}$	O_i+Mn_{Ca}	$O_i+Mn_{Ca}+V_{Ca}$	O_i	Mn_{Ca}
KCPO:0.23Mn	-767.80	-797.60	-782.50	10.22	18.92	-3.78	5.02

Table S6 The average bond lengths of Ca–O, Mn–O and Mg–O for KCMPO:0.23Mn^{2+}. (y = 0, 0.25, 0.4, 0.6, 0.7, 0.77).

	Ca–O (Å)	Mn–O (Å)	Mg–O (Å)
$y = 0$	2.38866	2.15086	—
$y = 0.25$	2.33512	2.41656	2.10998
$y = 0.4$	2.36500	2.23587	2.16382
$y = 0.6$	2.38954	2.18255	2.15658
$y = 0.7$	2.33936	2.44636	2.15835
$y = 0.77$	—	2.63382	2.17064

Table S7 The total Helmholtz free energies and formation energies of KCMPO:0.23Mn^{2+} (y = 0.4, 0.6, 0.77).

Samples	$E_{\text{tot-imperfect}}$ (eV)			E_f (eV)				
	$V_{Ca}+Mn_{Ca}+Mg_{Ca}$	$O_i+Mn_{Ca}+Mg_{Ca}$	$O_i+Mn_{Ca}+Mg_{Ca}+V_{Ca}$	Defect Complex		Point Defect		
				$O_i+Mn_{Ca}+Mg_{Ca}$	$O_i+Mn_{Ca}+Mg_{Ca}+V_{Ca}$	O_i	Mn_{Ca}	Mg_{Ca}
$y = 0.4$	-764.16	-789.41	-776.56	17.21	23.66	4.41	13.21	-0.09
$y = 0.6$	-762.50	-789.75	-774.62	16.47	25.2	4.07	12.87	1.07
$y = 0.77$	-761.80	-785.78	-774.12	19.64	25.3	8.04	16.84	8.04

References

1   B. Y. Qu, B. Zhang, L. Wang, R. L. Zhou and X. C. Zeng, *Chem. Mater.*, 2015, **27**, 2195–2202.
2   John P. Perdew, Kieron Burke and M. Ernzerhof, *Physiacal Review Letters*, 1996, **77**, 3865–3868.
3   Hendrik J. Monkhorst and J. D. Pack, *Phys. Rev. B*, 1976, **13**, 5188–5192.
4   L. E. Orgel, *J. Chem. Phys.*, 1955, **23**, 1004–1014.
5   L. Wu, B. Wang, Y. Zhang, L. Li, H. R. Wang, H. Yi, Y. F. Kong and J. J. Xu, *Dalton Trans.*, 2014, **43**, 13845–13851.
6   G. Blasse, *Phys. Lett. A*, 1968, **28**, 444–445.
7   D. L. Dexter and J. H. Schulman, *J. Chem. Phys.*, 1954, **22**, 1063–1070.
8   L. W. Wu, Y. X. Bai, L. Wu, H. Yi, X. Z. Zhang, L. X. Zhang, Y. F. Kong, Y. Zhang and J. J. Xu, *Dalton Trans.*, 2018, **47**, 13094–13105.
9   L. Wu, X. L. Chen, Y. P. Xu and Y. P. Sun, *Inorg. Chem.*, 2006, **45**, 3042–3047.
10 J. G. Cheng, P. L. Li, Z. J. Wang, Y. S. Sun, Q. Y. Bai, Z. L. Li, M. M. Tian, C. Wang and Z. P. Yang, *J. Mater. Chem. C*, 2017, **5**, 127–133.